Combined Leaderless Control of Translational, Shape-Preserving and Affine Multirobot Formations

Miguel Aranda, Rosario Aragüés and Gonzalo López-Nicolás

***Abstract*—This letter considers existing leaderless distributed controllers that achieve three types of planar multirobot formation. Concretely, these formations are equal to a reference configuration up to translation (type F1), shape-preserving transformation (type F2) and affine transformation (type F3). As contribution, we show that a linear combination of these controllers maintains their convergence properties, while also allowing specific control of the formation during the trajectory. This latter control is not possible when using the individual controllers separately, and is interesting in practical cases. As an example scenario, we study rotation-and-resizing formation maneuvers, where the goal is to achieve an F1 formation while remaining close to an F2 formation in the transient period. We show that, in this scenario, our combined controller produces trajectories approximating shortest-path shape-preserving maneuvers, which are desirable for efficiency and safety. We validate the controller in this and other scenarios using simulations and experiments with physical mobile robots.**

***Index Terms*—Multi-robot systems, distributed robot systems, autonomous agents.**

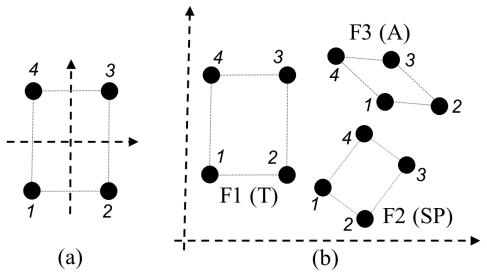

Fig. 1. (a): A reference formation of four robots. (b): Illustration of three types of formation (F1, F2, F3), equal to the reference one up to different types of geometric transformation: Translation (T), Shape-Preserving (SP) and Affine (A). In this letter, we consider three existing individual controller types that achieve F1, F2 and F3 formations, respectively. Our idea is to use a linear combination of these controllers. The resulting combined controller allows reaching a formation type while (unlike the individual controllers) controlling the formation type during the trajectory: for example, the team can reach an F1 formation while staying close to an F2 formation during the trajectory, or it can reach an F2 formation while staying close to an F3 one.

I. Introduction

MAINTAINING a formation is useful in multirobot tasks such as collective navigation, transport of an object, or monitoring of a phenomenon. Formation control [1] thus remains an important problem that has been addressed via various strategies [2]–[4]. A group of existing distributed formation control approaches (e.g., in [5]–[13]) rely on a core formulation where the control actions depend linearly on inter-robot relative positions. With these approaches, if robot interactions are captured by a static formation graph and a single-integrator robot model is considered, then the multirobot team's dynamics can be expressed via a constant Laplacian (or Laplacian-like) matrix.

In this letter, we consider three types of leaderless controllers in this group. Each type achieves asymptotically a planar formation of a corresponding type, which we call F1, F2 and F3. Given a reference configuration of the team, these types (illustrated in Fig. 1) consist in planar formations equal to that reference up to translation (F1), shape-preserving transformation (F2), and affine transformation (F3). The controllers we consider for F1 formations are based on a Laplacian matrix [5]–[7]; for F2 formations, they are based on a complex-valued Laplacian matrix or the equivalent real-valued matrix [8]–[10]; for F3 formations, they are based on a stress matrix [11]–[13].

We call these existing controllers *individual controllers*. What we propose in this letter is a *combined controller*, defined as a linear combination of individual ones for different formation types. When using the combined controller, the team will still reach a formation of type F1 or F2 asymptotically, while (unlike with the individual controllers) staying close to the other formation types (F2, F3) during the trajectory. This ability to accommodate multiple formation specifications is the most notable feature of the combined controller. Staying close to an F2 formation can, e.g., prevent damage to an object being transported [14], [15], and avoid inter-robot collisions during a task. Staying close to an F3 formation enables high flexibility in the team's configuration [12], [13] while still keeping an orderly layout of the robots that can facilitate their interactions.

We present a formal analysis of the combined controller based on the properties of the matrices associated with the individual controllers. Moreover, we study in depth a particular scenario: rotation-and-resizing maneuvers. In this scenario, our controller produces team trajectories that approximate shortest-path shape-preserving trajectories, which are desirable for efficiency and safety. Our approach is simple as it preserves the linear structure of the individual controllers, e.g., [5]–[13]. It is, however, more versatile than them in terms of the behaviors it can generate. We validate the combined controller in simulations with single-integrator agents and in experiments

This work was supported via projects PID2021-124137OB-I00 and TED2021-130224B-I00 funded by MCIN/AEI/10.13039/501100011033, by ERDF A way of making Europe and by the European Union NextGenerationEU/PRTR. It also received support via a María Zambrano fellowship funded by the Spanish Ministry of Universities and by the European Union-NextGenerationEU.

The authors are with Instituto de Investigación en Ingeniería de Aragón (I3A), Universidad de Zaragoza, Spain {miguel.aranda, raragues, gonlopez}@unizar.es

Digital Object Identifier (DOI): 10.1109/LRA.2023.3316889

with physical unicycle robots.

Next, we discuss related work where multiple formation controllers were combined. The studies [14]–[16] focused specifically on deformable object handling with a multirobot team. They used a core formation shape control term (F2) and added an affine formation term (F3) to gain closer control over the deformation during the task. Further terms were also employed to regulate the formation translation, rotation and scale. These studies considered a centralized setup (i.e., a complete formation graph). In comparison, here we focus on studying the general combination of existing distributed controllers and the problem of rotation-and-resizing maneuvers. The work [17] proposed a unification of formation controllers in a similar spirit to what we do here, with a leader-based scheme and a non-linear underlying formulation using sliding mode control. In [17], the unified controller was used by the leaders to make the full team achieve an affine, translational or rigid formation in finite time. In contrast, our combined controller is used by the full team in a leaderless approach, and it consists in a direct combination of linear controllers. In addition, we study specifically the trajectories for the case of rotation-and-resizing maneuvers. In [18], distance-based and barycentric coordinates-based controllers were combined to obtain a globally convergent rigid-formation controller. Our work encompasses more types of formations and studies formation maneuvers. The article [19] exploits double-integrator dynamics and combines distance-based and consensus controllers. Differently from our work, the resulting behavior is flocking with controlled shape.

We end the introduction with a discussion of multirobot maneuvering. This problem has most commonly been addressed using leader robots [12], [13], [20], [21], the principle being that the leaders' motions dictate the maneuver for the full team, and the follower robots adapt to the leaders' motions. Our approach enables leaderless maneuvers, which has the advantage of avoiding heavy reliance on leader performance. Leaderless maneuvers have been addressed using purposely designed mismatches in the formation's prescribed distances [2] and angles [22], or by modifying the complex-Laplacian coefficients [23]. Compared to [2], [22], [23], our work accommodates multiple formation types and focuses on the properties of the team's trajectories.

II. Problem setup

A. Notation and preliminary concepts

The norm $||\cdot||$ we use is the Euclidean one. The symbols $\mathbf{1}_n$ and $\mathbf{I}_n$ denote a column vector or n ones and the $n \times n$ identity matrix, respectively. $\otimes$ denotes the Kronecker product. We define $\mathbf{S} = [(0,1)^\intercal, (-1,0)^\intercal]$, i.e., a counterclockwise rotation of $\pi/2$ rad, and $\mathbf{T} = \mathbf{I}_n \otimes \mathbf{S} \in \mathbb{R}^{2n \times 2n}$. For a set of n points in the plane $\mathbf{v}_i \in \mathbb{R}^2$ for $i \in \mathcal{N} = \{1, ..., n\}$, we define the stack vector collecting them as $\mathbf{v} = [\mathbf{v}_1^\intercal, ..., \mathbf{v}_n^\intercal]^\intercal \in \mathbb{R}^{2n}$. $\mathbf{g_v}$ denotes the centroid of $\mathbf{v}$: $\mathbf{g_v} = (1/n)(\mathbf{1}_n \otimes \mathbf{I}_2)^\intercal \mathbf{v}$. $\mathbf{K} = (\mathbf{I}_n - (1/n)\mathbf{1}_n\mathbf{1}_n^\intercal) \otimes \mathbf{I}_2$ denotes a centering matrix such that $\mathbf{v}_z = \mathbf{K}\mathbf{v}$ denotes the translated version of $\mathbf{v}$ with zero centroid.

We consider a team of $n > 2$ robots lying on a planar, 2D space. We denote the robots' current positions, in a given fixed arbitrary reference frame, by a stack vector $\mathbf{q}(t) \in \mathbb{R}^{2n}$. The initial time for the control system is $t = 0$. We will sometimes omit the variable t, for compactness. The robot dynamics are assumed to be single-integrator, i.e., we have $\dot{\mathbf{q}} = \mathbf{u}$, where $\mathbf{u} = [\mathbf{u}_1^\intercal, ..., \mathbf{u}_n^\intercal]^\intercal \in \mathbb{R}^{2n}$ is the team control input for which we will design a control law. We define a static undirected formation graph $\mathcal{G} = (\mathcal{N}, \mathcal{E})$ to model the interactions between robots. Each vertex in $\mathcal{N}$ corresponds to a robot. An edge (i, j) in $\mathcal{E}$ means that the control law of robot i uses the relative position of j, and viceversa. Our work is based on the idea of reaching a desired formation of the team. For this, we define a reference configuration, or reference formation, by a set of n constant and distinct positions collected in $\mathbf{c} \in \mathbb{R}^{2n}$. For convenience and without loss of generality, we assume $\mathbf{g_c} = \mathbf{0}$. An example reference formation is shown in Fig. 1 (a).

B. Formation types

As already mentioned, we define three types of formation, all based on the reference configuration $\mathbf{c}$. We refer again to Fig. 1 for a graphical illustration. An F1 formation is equal to $\mathbf{c}$ up to translation. An F2 formation is equal to $\mathbf{c}$ up to a shape-preserving transformation consisting of translation, rotation and uniform scaling. An F3 formation is equal to $\mathbf{c}$ up to translation, rotation, arbitrary scaling in the two axes, and shearing; in other words, up to an affine transformation [12]. Let us formally define these formations. We consider that the team is in a formation of type Fi if the configuration $\mathbf{q}$ is in the set $\mathcal{S}_i$. The sets $\mathcal{S}_i$ are defined as

$$\mathcal{S}_1 = \{\mathbf{q} \in \mathbb{R}^{2n} : \mathbf{q} = \mathbf{c} + \mathbf{1}_n \otimes \mathbf{r},\ \mathbf{r} \in \mathbb{R}^2\}, \tag{1}$$

$$\mathcal{S}_2 = \{\mathbf{q} \in \mathbb{R}^{2n} : \mathbf{q} = (\mathbf{I}_n \otimes \mathbf{H})\mathbf{c} + \mathbf{1}_n \otimes \mathbf{r},\ \mathbf{r} \in \mathbb{R}^2, \ \mathbf{H} = [[h_1, h_2]^\intercal, [-h_2, h_1]^\intercal] \in \mathbb{R}^{2\times 2}\}, \tag{2}$$

$$\mathcal{S}_3 = \{\mathbf{q} \in \mathbb{R}^{2n} : \mathbf{q} = (\mathbf{I}_n \otimes \mathbf{G})\mathbf{c} + \mathbf{1}_n \otimes \mathbf{r},\ \mathbf{r} \in \mathbb{R}^2, \ \mathbf{G} \in \mathbb{R}^{2\times 2}\}. \tag{3}$$

Remark 1: We do not assume $\mathbf{H}$ and $\mathbf{G}$ to be invertible and, in particular, the definitions (2), (3) allow $\mathbf{H} = \mathbf{0}$ and $\mathbf{G} = \mathbf{0}$ respectively (which would correspond to achieving consensus). Note that this is also true for the individual controllers we consider [8]–[13]. The cases where these matrices are zero correspond to configurations having measure zero and do not occur in practice, as detailed in the cited references. Note that $\mathbf{H}$ in (2) encodes rotation and uniform scaling, as will be detailed in Sec. IV-A. As in [8]–[10], the F2 formations we consider, and hence the shape-preserving transformations we consider, do not include reflections.

C. Problem statement

The general problem we consider is designing a distributed controller $\mathbf{u}$ such that the multirobot team eventually reaches a formation of type F1 or F2. Within this general problem, the main focus of our work is on an additional, more specific goal: keeping the team close to a formation of a different type (F2 or F3) in the transient period. To this end, we will build upon existing individual controllers for F1, F2 and F3 formations, and propose a novel combination of them.

D. Supporting lemmas

We state two lemmas that are instrumental in supporting our approach. Although these lemmas are known results, we provide their proofs in the Appendix, for completeness.

Lemma 1: If $\mathbf{A} \in \mathbb{R}^{2n\times 2n}$ is symmetric negative semidefinite then under $\dot{\mathbf{q}} = \mathbf{A}\mathbf{q}$, $\mathbf{q}$ converges globally asymptotically to the orthogonal projection of $\mathbf{q}(0)$ onto $\ker(\mathbf{A})$.

Lemma 2: Given two symmetric negative semidefinite matrices $\mathbf{A} \in \mathbb{R}^{2n\times 2n}$ and $\mathbf{B} \in \mathbb{R}^{2n\times 2n}$, $\ker(\mathbf{A}+\mathbf{B}) = \ker(\mathbf{A}) \cap \ker(\mathbf{B})$.

III. Proposed combined formation controller

A. Individual controllers

We propose to use a linear combination of individual controllers of three types. Each type is designed to reach a formation of type F1, F2, F3, so we will use these same identifiers for the controller types. The controllers are designed for single-integrator dynamics. We denote them by $\mathbf{u}_{Fi} = \dot{\mathbf{q}}$ for $i \in \{1,2,3\}$, and express them as

$$\mathbf{u}_{F1} = \mathbf{A}_1(\mathbf{q}-\mathbf{c}), \tag{4}$$

$$\mathbf{u}_{F2} = \mathbf{A}_2\mathbf{q}, \tag{5}$$

$$\mathbf{u}_{F3} = \mathbf{A}_3\mathbf{q}. \tag{6}$$

$\mathbf{A}_1$, $\mathbf{A}_2$ and $\mathbf{A}_3 \in \mathbb{R}^{2n\times 2n}$ are constant (negated) Laplacian-like matrices associated with the underlying formation graph. $\mathbf{b} = -\mathbf{A}_1\mathbf{c} \in \mathbb{R}^{2n}$ in (4) represents a constant bias $\mathbf{b}_i \in \mathbb{R}^2$ for each robot i, determined by the relative positions of i's graph neighbors in the reference formation [5, Sec. I-D.6]. For uniformity when combining these controllers, we make $\mathbf{A}_1$, $\mathbf{A}_2$ and $\mathbf{A}_3$ have unit Euclidean norm, normalizing them. Next, we make two assumptions about these matrices.

Assumption 1: $\mathbf{A}_1$, $\mathbf{A}_2$ and $\mathbf{A}_3$ are symmetric negative semidefinite matrices.

Assumption 2: The kernels $\mathcal{K}_1 = \ker(\mathbf{A}_1)$, $\mathcal{K}_2 = \ker(\mathbf{A}_2)$ and $\mathcal{K}_3 = \ker(\mathbf{A}_3)$ are as follows:

$$\mathcal{K}_1 = \{\mathbf{q} \in \mathbb{R}^{2n} : \mathbf{q} = \mathbf{1}_n \otimes \mathbf{r},\ \mathbf{r} \in \mathbb{R}^2\}, \tag{7}$$

$$\mathcal{K}_2 = \mathcal{S}_2, \tag{8}$$

$$\mathcal{K}_3 = \mathcal{S}_3. \tag{9}$$

Notice the kernels $\mathcal{K}_i$ coincide with the sets $\mathcal{S}_i$, except for the $\mathbf{c}$ added for $\mathcal{S}_1$. There are existing controllers that have the proposed forms (4), (5), (6) and can satisfy Assumptions 1 and 2. Specifically, for $\mathbf{u}_{F1}$ we can use a consensus-based formation controller [5], [6], which achieves an F1 formation. For $\mathbf{u}_{F2}$ we can use a formation controller based on a complex Laplacian (or an analogous formulation) [8]–[10], which achieves an F2 formation. For $\mathbf{u}_{F3}$ we can use an affine formation controller [11], which achieves an F3 formation.

We assume the formation graphs for the individual controllers are static and undirected, and we denote them by $\mathcal{G}_1 = (\mathcal{N}, \mathcal{E}_1)$ for $\mathbf{u}_{F1}$, $\mathcal{G}_2 = (\mathcal{N}, \mathcal{E}_2)$ for $\mathbf{u}_{F2}$ and $\mathcal{G}_3 = (\mathcal{N}, \mathcal{E}_3)$ for $\mathbf{u}_{F3}$. The graph requirements are different for different formation types. Examples of these requirements are: connectedness for F1, rigidity-related constraints for F2, and universal rigidity for F3. Requirements also vary for different controllers within a formation type.

B. Proposed combined controller

As mentioned, we propose a combined controller, defined as a linear combination of the individual controllers:

$$\mathbf{u} = w_1\mathbf{u}_{F1} + w_2\mathbf{u}_{F2} + w_3\mathbf{u}_{F3}, \tag{10}$$

where $w_1 \geq 0$, $w_2 \geq 0$, $w_3 \geq 0$ are scalar weights. Notice that, from Assum. 2, $\mathbf{c}$ is in $\mathcal{K}_2$ and $\mathcal{K}_3$. Therefore, $\mathbf{A}_2\mathbf{c} = \mathbf{A}_3\mathbf{c} = \mathbf{0}$ and we can express equivalently (10) as

$$\mathbf{u} = \mathbf{A}(\mathbf{q}-\mathbf{c}),\ \text{with}\ \mathbf{A} = w_1\mathbf{A}_1 + w_2\mathbf{A}_2 + w_3\mathbf{A}_3. \tag{11}$$

From Assum. 1, $\mathbf{A}$ is symmetric negative semidefinite. Let us denote $\mathcal{K}_A = \ker(\mathbf{A})$. Observe from expressions above that $\mathcal{K}_1 \subset \mathcal{K}_2 \subset \mathcal{K}_3$. Using this and Lemma 2, it is clear that if $w_1 > 0$, $\mathcal{K}_A = \mathcal{K}_1$, and if $w_1 = 0$ and $w_2 > 0$, $\mathcal{K}_A = \mathcal{K}_2$.

C. Implementing the combined controller

As $\mathbf{A}_1$, $\mathbf{A}_2$ and $\mathbf{A}_3$ have a Laplacian-like structure, the individual controllers [5], [6], [8]–[11] and hence, the combined one (10), (11) too, can be implemented by every robot i using the relative positions, $\mathbf{q}_j - \mathbf{q}_i$, of its graph neighbors j. Robot i can compute its control $\mathbf{u}_i$ by measuring, via sensing or communications, these relative positions at run time, and applying the corresponding coefficients from the matrices and the bias $\mathbf{b}_i$. As implementing the combined controller requires the capability to implement the individual ones, we assume $\mathcal{G}$ is such that $\mathcal{E}_1 \subseteq \mathcal{E}$ (if $w_1 > 0$), $\mathcal{E}_2 \subseteq \mathcal{E}$ (if $w_2 > 0$) and $\mathcal{E}_3 \subseteq \mathcal{E}$ (if $w_3 > 0$). Each individual controller (i) has its own minimum required number of graph edges and (ii) can still be implemented with more edges than the minimum. For simplicity and resource efficiency, one option is to use the same graph for all individual controllers, chosen as the graph with most edges among the graphs required for each individual controller. We do this in our tests (Sec. V).

Note that the controller does not need absolute position measurements. For an F1 controller, the robots have to express their relative position measurements with respect to a common reference of orientation [1]. For F2 and F3 controllers, the robots do not need a common reference of orientation as long as they measure relative positions expressed in their own coordinate frames, as noted, e.g., in [8]–[10], [12].

D. Analysis and types of behavior

Lemma 3: If Assumptions 1 and 2 hold, under controller (11) with $w_1 \geq 0$, $w_2 \geq 0$, $w_3 \geq 0$, the centroid $\mathbf{g_q}$ is invariant. This holds for any $\mathbf{c}$, including $\mathbf{c} = \mathbf{0}$.

Proof: The centroid dynamics is $\dot{\mathbf{g}}_\mathbf{q} = (1/n)(\mathbf{1}_n \otimes \mathbf{I}_2)^\intercal\dot{\mathbf{q}} = (1/n)(\mathbf{1}_n \otimes \mathbf{I}_2)^\intercal\mathbf{A}(\mathbf{q}-\mathbf{c})$. Note in this expression that $((\mathbf{1}_n\otimes\mathbf{I}_2)^\intercal\mathbf{A})^\intercal = \mathbf{A}(\mathbf{1}_n\otimes\mathbf{I}_2) = [\mathbf{A}(\mathbf{1}_n\otimes[1,0]^\intercal), \mathbf{A}(\mathbf{1}_n\otimes[0,1]^\intercal)]$. Clearly, $\mathbf{1}_n\otimes[1,0]^\intercal$ and $\mathbf{1}_n\otimes[0,1]^\intercal$ are in $\mathcal{K}_1$, $\mathcal{K}_2$ and $\mathcal{K}_3$. Therefore, they are in $\mathcal{K}_A$. This means $\mathbf{A}(\mathbf{1}_n \otimes \mathbf{I}_2) = \mathbf{0}$, i.e., $(\mathbf{1}_n \otimes \mathbf{I}_2)^\intercal\mathbf{A} = \mathbf{0}$. Hence, $\dot{\mathbf{g}}_\mathbf{q} = \mathbf{0}$. ■

Theorem 1: If Assumptions 1 and 2 hold, under the combined controller (11), (i) if $w_1 = 0$, $w_2 > 0$, $w_3 \geq 0$, $\mathbf{q}$ converges globally asymptotically to an F2 formation equal to the orthogonal projection of $\mathbf{q}(0)$ onto $\mathcal{K}_2$; and (ii) if $w_1 > 0$, $w_2 \geq 0$, $w_3 \geq 0$, $\mathbf{q}$ converges globally asymptotically to the F1 formation $\mathbf{c} + \mathbf{1}_n \otimes \mathbf{g_q}(0)$.

Proof: (i) $\mathbf{u} = w_2\mathbf{u}_{F2}+w_3\mathbf{u}_{F3} = \mathbf{A}\mathbf{q}$ with $\mathbf{A} = w_2\mathbf{A}_2+ w_3\mathbf{A}_3$. As seen above, $\mathbf{A}$ is symmetric negative semidefinite and $\mathcal{K}_A = \mathcal{K}_2$ in this case. Therefore, from Lemma 1, under $\dot{\mathbf{q}} = \mathbf{u} = \mathbf{A}\mathbf{q}$, $\mathbf{q}$ converges globally asymptotically to the orthogonal projection of $\mathbf{q}(0)$ onto $\mathcal{K}_2$.

(ii) We have $\mathcal{K}_A = \mathcal{K}_1$ in this case. Let us first consider the dynamics without the constant term $\mathbf{c}$, i.e., $\dot{\mathbf{q}} = \mathbf{A}\mathbf{q}$. Due to centroid invariance (Lemma 3) and to Lemma 1, all the robots converge to the initial centroid. Notice that this implies that $\mathbf{A}$ is such that $\lim_{t\to\infty} \mathbf{e}^{\mathbf{A}t}\mathbf{v} = \mathbf{1}_n \otimes \mathbf{g}_\mathbf{v}$ for any $\mathbf{v} \in \mathbb{R}^{2n}$. Then, consider the trajectory of the actual system $\dot{\mathbf{q}} = \mathbf{u} = \mathbf{A}(\mathbf{q}-\mathbf{c})$, which is $\mathbf{q}(t) = \mathbf{c}+\mathbf{e}^{\mathbf{A}t}(\mathbf{q}(0)-\mathbf{c})$. As the centroid of $\mathbf{c}$ is zero, the centroid of $(\mathbf{q}(0) - \mathbf{c})$ is $\mathbf{g}_\mathbf{q}(0)$. Therefore, $\lim_{t\to\infty} \mathbf{q}(t) = \mathbf{c} + \mathbf{1}_n \otimes \mathbf{g}_\mathbf{q}(0)$, as stated. ■

Thm. 1 shows that the combined controller ensures formation convergence. In addition, a key feature is that it allows further control of the formation during the trajectory. Specifically, the behaviors enabled by this controller are:

1) If $w_1 > 0$, $w_2 > 0$, $w_3 = 0$: convergence to an F1 formation while staying close to an F2 formation.
2) If $w_1 = 0$, $w_2 > 0$, $w_3 > 0$: convergence to an F2 formation while staying close to an F3 formation.
3) If $w_1 > 0$, $w_2 = 0$, $w_3 > 0$: convergence to an F1 formation while staying close to an F3 formation.
4) If $w_1 > 0$, $w_2 > 0$, $w_3 > 0$: convergence to an F1 formation while staying close to an F2 formation and to an F3 formation.

These behaviors are illustrated in our validation (Sec. V). As can be reasoned intuitively, the team will stay closer to an Fi formation if one increases w_i. Behavior 1) in the specific case of a formation maneuver, for which the initial configuration is an F2 formation and not any arbitrary configuration, is studied in detail in Sec. IV. An interesting fact to highlight is that the combined controller does not alter the final configuration. Indeed, from Thm. 1, the final configuration depends only on the initial one, $\mathbf{q}(0)$. For a given $\mathbf{q}(0)$, if $w_1 > 0$ the individual controller $\mathbf{u}_{F1}$ and any of the combined ones converge to an identical F1 formation; and if $w_1 = 0$, $w_2 > 0$, the individual controller $\mathbf{u}_{F2}$ and the combined one converge to an identical F2 formation.

IV. Example scenario: Formation maneuvers

This section studies a relevant scenario where the application of the combined controller provides important advantages: executing a formation maneuver to reach an F1 formation from an initial F2 formation. For this, we will use $\mathbf{A} = w_1\mathbf{A}_1 + w_2\mathbf{A}_2$, i.e., we take $w_3 = 0$. We start by introducing some necessary concepts.

A. Shape-preserving transformation and optimal formation

Consider the class of 2×2 real matrices with equal diagonal entries and opposite off-diagonal entries:

$$\mathbf{M} = \begin{bmatrix} m_1 & -m_2 \\ m_2 & m_1 \end{bmatrix}, \text{ with } m_1,\, m_2 \in \mathbb{R}. \tag{12}$$

Assumption 3: $\mathbf{A}_1$ and $\mathbf{A}_2$ are block matrices $\mathbf{A}_1 = [\mathbf{A}_{ij_1}]$, $\mathbf{A}_2 = [\mathbf{A}_{ij_2}]$, $\forall i \in \mathcal{N}$, $\forall j \in \mathcal{N}$, such that every block of size 2×2 $\mathbf{A}_{ij_1}$, $\mathbf{A}_{ij_2}$ has the form (12).

This assumption is satisfied by the matrices used in the controllers for F1 [5], [6] and F2 [8]–[10] formations. With standard manipulations one can see that the property stated in Assum. 3 is preserved under linear combinations and products. Hence, $\mathbf{A}^k$ for every integer $k \geq 0$ satisfies the property. Notice the class (12) includes the zero 2×2 matrix. Consider now a nonzero matrix $\mathbf{H}$ with the same form:

$$\mathbf{H} = \begin{bmatrix} h_1 & -h_2 \\ h_2 & h_1 \end{bmatrix}, \text{ with } h_1,\, h_2 \in \mathbb{R},\, h_1^2 + h_2^2 > 0. \tag{13}$$

For a vector $\mathbf{x} \in \mathbb{R}^{2n}$ of n point positions with zero centroid, $\mathbf{x}_H = (\mathbf{I}_n \otimes \mathbf{H})\mathbf{x} \in \mathbb{R}^{2n}$ is a vector of n point positions with zero centroid and which are rotated (by $\theta \in (-\pi, \pi]$) and uniformly scaled (by $s \in \mathbb{R}_{>0}$) relative to $\mathbf{x}$, since

$$\mathbf{H} = s \begin{bmatrix} \cos(\theta) & -\sin(\theta) \\ \sin(\theta) & \cos(\theta) \end{bmatrix}, \text{ with } \begin{cases} s = \sqrt{h_1^2 + h_2^2} \\ \theta = \text{atan2}(h_2, h_1). \end{cases}$$

A transformation of the form (13) is *shape-preserving*, because rotation and uniform scaling actions do not change a shape. Now, let us define the *optimal F2 formation*, $\mathbf{p}$, as the closest (in norm) configuration to $\mathbf{q}$ where the team is in an F2 formation. Referring to (2), to determine $\mathbf{p}$ we need to compute the optimal translation and the optimal transformation of $\mathbf{c}$ with the form (12). The optimal translation is the one that makes the centroid equal to the centroid of $\mathbf{q}$, $\mathbf{g}_\mathbf{q}$ [10]. All through Sec. IV, we consider, without loss of generality, that $\mathbf{g}_\mathbf{q}(t) = \mathbf{0}\ \forall t$; more details are given in Sec. IV-F. Hence, the centroid of $\mathbf{p}$ is zero. In addition, the optimal transformation matrix is [10]

$$\mathbf{H}_g = \begin{bmatrix} h_{1g} & -h_{2g} \\ h_{2g} & h_{1g} \end{bmatrix}, \ h_{1g} = \frac{\mathbf{q}^\intercal\mathbf{c}}{\mathbf{c}^\intercal\mathbf{c}}, \ h_{2g} = \frac{\mathbf{q}^\intercal\mathbf{T}\mathbf{c}}{\mathbf{c}^\intercal\mathbf{c}}, \tag{14}$$

where $\mathbf{H}_g$, if it is nonzero, is a shape-preserving transformation (13). The optimal F2 formation is, hence,

$$\mathbf{p}(t) = (\mathbf{I}_n \otimes \mathbf{H}_g(t))\mathbf{c}. \tag{15}$$

Since $(\mathbf{I}_n \otimes \mathbf{H}_g)\mathbf{c} = h_{1g}\mathbf{c} + h_{2g}\mathbf{T}\mathbf{c}$, using (14) we have

$$\mathbf{p} = h_{1g}\mathbf{c} + h_{2g}\mathbf{T}\mathbf{c} = \frac{\mathbf{q}^\intercal\mathbf{c}}{\mathbf{c}^\intercal\mathbf{c}}\mathbf{c} + \frac{\mathbf{q}^\intercal\mathbf{T}\mathbf{c}}{\mathbf{c}^\intercal\mathbf{c}}\mathbf{T}\mathbf{c}. \tag{16}$$

Now, we can use the facts that $(\mathbf{q}^\intercal\mathbf{c})\mathbf{c} = \mathbf{c}\mathbf{c}^\intercal\mathbf{q}$ and $(\mathbf{q}^\intercal\mathbf{T}\mathbf{c})\mathbf{T}\mathbf{c} = \mathbf{T}\mathbf{c}\mathbf{c}^\intercal\mathbf{T}^\intercal\mathbf{q}$ to obtain

$$\mathbf{p}(t) = \frac{\mathbf{c}\mathbf{c}^\intercal + \mathbf{T}\mathbf{c}\mathbf{c}^\intercal\mathbf{T}^\intercal}{\mathbf{c}^\intercal\mathbf{c}}\mathbf{q}(t). \tag{17}$$

This useful expression relates $\mathbf{p}$ and $\mathbf{q}$ linearly and will be exploited in our analysis presented in subsequent sections.

B. Definition of a maneuver

We define a *rotation-and-resizing maneuver* (or, simply, a *maneuver*) as a trajectory of the multirobot system moving from a *beginning* ($\mathbf{c}^b$) to an *ending* ($\mathbf{c}^e$) configuration, both having the same centroid, and both having the same shape as $\mathbf{c}$. We define the configurations as $\mathbf{c}^b = (\mathbf{I}_n \otimes \mathbf{H}_b)\mathbf{c}$, $\mathbf{c}^e = (\mathbf{I}_n \otimes \mathbf{H}_e)\mathbf{c}$, where $\mathbf{H}_b$ and $\mathbf{H}_e$ have the form (13). Without loss of generality, we specifically take $\mathbf{H}_e = \mathbf{I}_2$, i.e., $\mathbf{c}^e = \mathbf{c}$. Therefore, $\mathbf{c}^b$ is an F2 formation and $\mathbf{c}^e$ is an F1 formation.

In concrete terms, for a generic variable representing n positions $\mathbf{x} \in \mathbb{R}^{2n}$, a maneuver is a trajectory $\mathbf{x}(t)$ such that $\mathbf{x}(0) = \mathbf{c}^b$ and $\lim_{t\to\infty} \mathbf{x}(t) = \mathbf{c}$. We disregard *antipodal* maneuvers, i.e., those for which $\mathbf{H}_e = \kappa \mathbf{H}_b$ for a $\kappa < 0$. Such extreme maneuvers can be accomplished by dividing them into a sequence of smaller sub-maneuvers.

C. Shortest-path shape-preserving maneuvers

Next, we give our definitions of two relevant properties a maneuver can have. A maneuver is *shortest-path* if every robot moves along a straight line, and never reverses direction. A maneuver is *shape-preserving* if the team keeps the same shape, i.e., $\mathbf{x}_z(t) = (\mathbf{I}_n \otimes \mathbf{H}(t))\mathbf{c}\ \forall t \geq 0$, with $\mathbf{H}(t)$ of the form (13). Shortest-path maneuvers are efficient as their associated energy consumption is low. Shape-preserving maneuvers make it easier to ensure safety, as the relative positions of every pair of robots evolve in a tightly coordinated way. We are interested in a class of maneuvers that satisfy the two discussed properties at once. This class is defined by the following set of trajectories of $\mathbf{x}$:

$$\mathbf{x}(t) = \beta(t)(\mathbf{c}^b - \mathbf{c}) + \mathbf{c}, \ \ t \geq 0, \tag{18}$$

where $\beta(t) \in \mathbb{R}$ satisfies the following three conditions:

$$\beta(0) = 1, \ \lim_{t\to\infty} \beta(t) = 0, \ \beta(t_b) \leq \beta(t_a)\ \forall t_b > t_a \geq 0. \tag{19}$$

Notice that (18) is a convex combination that represents a line joining $\mathbf{c}^b$ and $\mathbf{c}$.

Proposition 1: Any trajectory having the form defined by (18)-(19) is a shortest-path shape-preserving maneuver.

Proof: The trajectory is shortest-path as, for robot i,

$$\mathbf{x}_i(t) = \beta(t)(\mathbf{c}_i^b - \mathbf{c}_i) + \mathbf{c}_i, \ \ \beta(t) \in [0,1]\ \ \forall t \geq 0, \tag{20}$$

and since $\beta(t)$ cannot increase as time progresses, the motion is always forwards (i.e., towards $\mathbf{c}_i$). To see that the maneuver is shape-preserving, we express (18) as

$$\mathbf{x}(t) = \beta(t)\big((\mathbf{I}_n \otimes \mathbf{H}_b)\mathbf{c} - \mathbf{c}\big) + \mathbf{c} = \big(\mathbf{I}_n \otimes \mathbf{H}_\beta(t)\big)\mathbf{c}, \tag{21}$$

where $\mathbf{H}_\beta(t) = (1 - \beta(t))\mathbf{I}_2 + \beta(t)\mathbf{H}_b$. Notice $\mathbf{g}_\mathbf{x}(t) = \mathbf{0}$, i.e., $\mathbf{x}_z(t) = \mathbf{x}(t), \forall t \geq 0$. One can see that $\mathbf{H}_\beta(t)$ can only become zero if the maneuver is antipodal, a case we disregarded. Therefore, $\mathbf{H}_\beta(t)$ has the form (13) and, from the definition above, the maneuver is shape-preserving. ■

D. Maneuvering using the combined controller

Next, we show that using (11) for maneuvering, (i) the trajectory of the optimal F2 formation $\mathbf{p}$ is a maneuver of the class defined by (18)-(19) and (ii) the trajectory of the team, $\mathbf{q}$, can approximate the trajectory of $\mathbf{p}$.

1) Trajectory of $\mathbf{p}$*:* We give an auxiliary result (Prop. 2, proven in the Appendix), and then the main result (Thm. 2).

Proposition 2: If Assumptions 1, 2 and 3 hold and $w_1 > 0$, $w_2 \geq 0$, $w_3 = 0$, then: (i) $\mathbf{c}^\intercal e^{\mathbf{A}t}\mathbf{T}\mathbf{c} = (\mathbf{T}\mathbf{c})^\intercal e^{\mathbf{A}t}\mathbf{c} = 0$, and (ii) $(\mathbf{T}\mathbf{c})^\intercal e^{\mathbf{A}t}\mathbf{T}\mathbf{c} = \mathbf{c}^\intercal e^{\mathbf{A}t}\mathbf{c}$.

Theorem 2: If Assumptions 1, 2 and 3 hold and $\mathbf{q}(0) = \mathbf{c}^b$, under controller (11) with $w_1 > 0$, $w_2 \geq 0$, $w_3 = 0$, the trajectory of $\mathbf{p}$ is a shortest-path shape-preserving maneuver with the form

$$\mathbf{p}(t) = \beta_p(t)(\mathbf{c}^b - \mathbf{c}) + \mathbf{c}, \ \text{ with } \ \beta_p(t) = \frac{\mathbf{c}^\intercal e^{\mathbf{A}t}\mathbf{c}}{\mathbf{c}^\intercal\mathbf{c}}. \tag{22}$$

Proof: We first substitute in the expression of $\mathbf{p}$ (17) the trajectory of $\mathbf{q}$ under $\dot{\mathbf{q}} = \mathbf{A}(\mathbf{q} - \mathbf{c})$, taking $\mathbf{q}(0) = \mathbf{c}^b$:

$$\mathbf{p}(t) = \frac{\mathbf{c}\mathbf{c}^\intercal + \mathbf{T}\mathbf{c}\mathbf{c}^\intercal\mathbf{T}^\intercal}{\mathbf{c}^\intercal\mathbf{c}}(e^{\mathbf{A}t}(\mathbf{c}^b - \mathbf{c}) + \mathbf{c}). \tag{23}$$

Defining $\mathbf{H}_b = [(h_{1b}, h_{2b})^\intercal, (-h_{2b}, h_{1b})^\intercal]$, notice that we have $\mathbf{c}^b = h_{1b}\mathbf{c} + h_{2b}\mathbf{T}\mathbf{c}$. We substitute $\mathbf{c}^b - \mathbf{c} = (h_{1b} - 1)\mathbf{c} + h_{2b}\mathbf{T}\mathbf{c}$ in (23). As $(\mathbf{T}\mathbf{c})^\intercal\mathbf{c} = \mathbf{0}$, we have

$$\begin{aligned}\mathbf{p}(t) = &\frac{1}{\mathbf{c}^\intercal\mathbf{c}}\Big[\mathbf{c}\Big((h_{1b} - 1)\mathbf{c}^\intercal e^{\mathbf{A}t}\mathbf{c} + h_{2b}\mathbf{c}^\intercal e^{\mathbf{A}t}\mathbf{T}\mathbf{c} + \mathbf{c}^\intercal\mathbf{c}\Big)\\ &+ \mathbf{T}\mathbf{c}\Big((h_{1b} - 1)(\mathbf{T}\mathbf{c})^\intercal e^{\mathbf{A}t}\mathbf{c} + h_{2b}(\mathbf{T}\mathbf{c})^\intercal e^{\mathbf{A}t}\mathbf{T}\mathbf{c}\Big)\Big].\end{aligned}$$

Using Prop. 2, one directly finds the trajectory (22). Let us now show (22) is a shortest-path shape-preserving maneuver. Notice $\dot{\beta}_p(t) = \frac{1}{\mathbf{c}^\intercal\mathbf{c}}\frac{d}{dt}(\mathbf{c}^\intercal e^{\mathbf{A}t}\mathbf{c}) = \frac{1}{\mathbf{c}^\intercal\mathbf{c}}\mathbf{c}^\intercal\mathbf{A}e^{\mathbf{A}t}\mathbf{c}$. Recall $\mathbf{A}$ is symmetric negative semidefinite from Assum. 1, and note $e^{\mathbf{A}t}$ is symmetric positive definite as $\mathbf{A}$ is symmetric. Hence, as $\mathbf{A}$ and $e^{\mathbf{A}t}$ clearly commute, we conclude $\mathbf{A}e^{\mathbf{A}t}$ is symmetric negative semidefinite. Therefore, $\dot{\beta}_p(t) \leq 0$. Also, as seen in the proof of Thm. 1, part (ii), $\mathbf{A}$ is such that $\lim_{t\to\infty} \mathbf{e}^{\mathbf{A}t}\mathbf{v} = \mathbf{1}_n \otimes \mathbf{g}_\mathbf{v}$ for any $\mathbf{v} \in \mathbb{R}^{2n}$. This implies $e^{\mathbf{A}t}\mathbf{c}$ converges to zero asymptotically, and therefore $\lim_{t\to\infty} \beta_p(t) = 0$. Note, then, that $\beta_p(t)$ satisfies $\beta_p(0) = 1$, $\dot{\beta}_p(t) \leq 0$, and $\lim_{t\to\infty} \beta_p(t) = 0$. Hence, (22) is of the class defined by (18)-(19) and, from Prop. 1, it is a shortest-path shape-preserving maneuver. ■

2) Trajectory of $\mathbf{q}$*:* To quantify how closely $\mathbf{q}(t)$ approximates $\mathbf{p}(t)$, we express the error between the two next.

Proposition 3: If Assumptions 1, 2 and 3 hold and $\mathbf{q}(0) = \mathbf{c}^b$, under control (11) with $w_1 > 0$, $w_2 \geq 0$, $w_3 = 0$, $\mathbf{q}$ converges asymptotically to $\mathbf{c}$ and its error relative to $\mathbf{p}$ is

$$\mathbf{e}(t) = \mathbf{q}(t) - \mathbf{p}(t) = \left(e^{\mathbf{A}t} - \frac{\mathbf{c}^\intercal e^{\mathbf{A}t}\mathbf{c}}{\mathbf{c}^\intercal\mathbf{c}}\mathbf{I}_{2n}\right)(\mathbf{c}^b - \mathbf{c}), \tag{24}$$

with $\mathbf{e}(0) = \mathbf{0}$ and $\lim_{t\to\infty} \mathbf{e}(t) = \mathbf{0}$.

Proof: $\mathbf{q}$ converging to $\mathbf{c}$ follows from Thm. 1, part (ii). One gets (24) by using (22) and the trajectory $\mathbf{q}(t)$ when $\mathbf{q}(0) = \mathbf{c}^b$. $\mathbf{e}(0) = \mathbf{0}$ follows directly from (24). $\lim_{t\to\infty} \mathbf{e}(t) = \mathbf{0}$ follows from noticing that $\mathbf{p}(t)$ is a maneuver (Thm. 2) and therefore $\mathbf{p}$ converges to $\mathbf{c}$. ■

E. Effect of the weights w_1, w_2

Ideally, we would like to maintain $\mathbf{e}(t)$ at zero during the trajectory. This can be achieved by choosing $w_1 = 0$. However, $w_1 = 0$ is not a feasible choice: it implies the robots remain static, as $\mathbf{q}(0) = \mathbf{c}^b$ is an F2 formation and hence the F2 control term, for any $w_2 \geq 0$, produces no motion. With $w_1 > 0$, $w_2 > 0$, as $w_2/w_1 \to \infty$ makes $\mathbf{e}(t) \to \mathbf{0}$ we can reduce $||\mathbf{e}(t)||$ during the trajectory by choosing a higher ratio w_2/w_1. This strengthens shape preservation (i.e., closeness to an F2 formation). In choosing w_1 and w_2 to increase w_2/w_1, one should take into account that reducing w_1 makes the advancement towards $\mathbf{c}$ slower, while increasing w_2 makes the behavior more sensitive to perturbations. An important point

is that our expression (24) can be readily used at the design stage to choose w_1 and w_2 to fit given specifications. We leave a deeper treatment of design considerations for future work.

F. Centroid preservation and team translation

Recall the centroid $\mathbf{g_q}$ is invariant under our controller (Lem. 3) and, hence, during a maneuver. Preserving the centroid is advantageous for rotation-and-resizing maneuvers: it reduces the area occupied by the team and the distances traveled by the robots during the motion. Achieving a motion involving rotation, resizing and translation is possible by adding a translation control term to the controller we propose. Another point to note is we used $\mathbf{c}^b$ and $\mathbf{c}^e$ with zero centroid for simplicity of exposition, but the centroid can have any value. If $\mathbf{g_q} = \mathbf{g}_{\mathbf{c}^b} = \mathbf{g}_{\mathbf{c}^e}$ is nonzero, we can express $\mathbf{q} = \mathbf{q}_z + \mathbf{1}_n \otimes \mathbf{g_q}$ (and analogously for $\mathbf{c}^b$ and $\mathbf{c}^e$). Clearly $\mathbf{1}_n \otimes \mathbf{g_q}$ is in $\mathcal{K}_A$, so the controller produces the same motion considering either $\mathbf{q}$ or the zero-centroid $\mathbf{q}_z$.

V. Experimental validation

We present results from several scenarios. A **video** of our tests is also provided as supplementary material. As $\mathbf{u}_{F1}$ we use a standard Laplacian-based controller [5, eq. 6]. As $\mathbf{u}_{F2}$ we use the controller [10, eq. 11], which is based on a graph structured in triads. As $\mathbf{u}_{F3}$ we use the controller [11, eq. 2]. We remark that other controllers (satisfying Assumptions 1, 2 and 3) can be used. We define the following distance functions that will be useful to illustrate the performance:

$$\begin{aligned} d_1(t) &= ||(\mathbf{I}_{2n} - \mathbf{P}_1)\mathbf{q}(t) - \mathbf{c}||, \\ d_2(t) &= ||(\mathbf{I}_{2n} - \mathbf{P}_2)\mathbf{q}(t)||, \\ d_3(t) &= ||(\mathbf{I}_{2n} - \mathbf{P}_3)\mathbf{q}(t)||. \end{aligned} \tag{25}$$

$\mathbf{P}_i$ denotes the orthogonal projection matrix onto $\mathcal{K}_i$. Hence, $d_i(t)$ expresses the distance from $\mathbf{q}(t)$ to an Fi formation. As $\mathbf{p}(t)$ is the closest (in norm) F2 formation to $\mathbf{q}_z(t)$ (Sec. IV-A), we can also express $d_2(t) = ||\mathbf{q}_z(t) - \mathbf{p}(t)||$. Hence, $d_2(t) = ||\mathbf{e}(t)||$, noting that one should use $\mathbf{q}_z(t)$ instead of $\mathbf{q}(t)$ in (24) if the centroid of $\mathbf{q}(t)$ is not zero.

A. Simulation

We first validate our method in three simulation scenarios run in MATLAB for a seven-robot formation. The results are illustrated in Fig. 2. The reference formation with numbered robots is illustrated in top-left of the figure. The graph we consider for all controllers is the same: $\mathcal{G} = \mathcal{G}_i$ with $i = 1$, 2 and 3 with edge set $\mathcal{E} = \{(1,2),(1,3),(2,3),(2,4),...,(6,7),(6,1),(7,1),(7,2)\}$. The robots are single integrators and we use controller (11).

Scenario 1 is a rotation-and-resizing maneuver (Sec. IV). We use $w_1 = 0.4$, $w_2 = 20$, $w_3 = 0$, and $\mathbf{c}^b = s_b\mathbf{R}_b(\theta_b)\mathbf{c}$ with $s_b = 1.3$, $\theta_b = -80$ deg. We compare the performance with the individual F1 controller. Notice d_1 evolves similarly in the two cases. Some robots have equal velocity norm due to symmetry. The combined controller produces shorter paths and, as shown by d_2, it keeps the team closer to an F2 formation. Testing with w_2 equal to $0, 1, 10, 20, 50$ and 100 we obtain peak values of d_2 of $0.51, 0.31, 0.12, 0.07, 0.04$ and 0.02 m respectively, i.e., a higher w_2 reduces d_2.

Scenarios 2 and 3, discussed next, illustrate the results of Sec. III. In scenario 2, we consider reaching an F2 formation starting from an F3 formation. We choose $w_1 = 0$, $w_2 = 5$, $w_3 = 70$. This time, the combined controller eventually reaches an F2 formation while the team configuration stays close to an affine transformation of $\mathbf{c}$ (i.e., an F3 formation): this allows maintaining an orderly arrangement of the robots during the motion. We also test the individual F2 controller, for which the peak value of d_3 over time is 0.27 m. This is reduced to 0.06 m when using the combined controller.

In scenario 3, we consider a deformed initial shape and we use $w_1 = 1$, $w_2 = 10$, $w_3 = 10$, i.e., we combine all three controllers. We compare again the individual F1 controller and the combined one. We use velocity saturation so that the maximum velocity is the same for the two controllers. Without saturation, the maximum norm of the initial velocity among all robots with the combined controller would be 2.08 m/s. The evolution of d_1 is similar for both controllers but, as expected, the team stays closer to F2 and F3 formations with the combined controller, as the d_2 and d_3 curves illustrate. Indeed, the individual controller reduces d_2 to 5% of its initial value in 16.06 sec, whereas with the combined controller this occurs considerably faster (2.62 sec), i.e., the team gets close to the desired shape early on and remains close to it thereafter, not allowing unpredictable shape evolutions.

B. Experiments with physical robots

Finally, we report tests done in the Robotarium [24] with a team of six mobile robots executing a rotation-and-resizing maneuver (Sec. IV). The results are illustrated in Fig. 3. We choose $\mathbf{c}^b = s_b\,\mathbf{R}_b(\theta_b)\,\mathbf{c}$ with $s_b = 0.8$, $\theta_b = -60$ deg. We run two tests using (11), one with the individual F1 controller ($w_1 = 1.6$, $w_2 = 0$, $w_3 = 0$) and the other with the combined controller ($w_1 = 0.8$, $w_2 = 8$, $w_3 = 0$). We use the same graph (see bottom-left of Fig. 3) for both tests. The weights chosen provide a similar convergence time in both cases. As the robots are unicycles, the single-integrator velocities of our controllers are transformed into the corresponding linear (v) and angular (ω) unicycle velocities by the Robotarium's own conversion algorithms. In the two tests, all the robots have the same heading initially. Moreover, we make them all stop moving when the errors associated with both d_1 and d_2 fall below a certain threshold.

Observing intermediary configurations during the task, one notices that the individual controller ($w_2 = 0$) fails to preserve the shape during the motion and causes a considerable deformation. This is also manifested by the evolution of d_2. This fact would be problematic for certain applications such as object manipulation. In comparison, the proposed combined controller preserves the shape much more closely. It also uses lower velocities and shorter paths to complete the task. Even though the unicycle kinematic constraints have a visible effect on the obtained motions, the core features of the proposed single-integrator controller are maintained. Thus, these tests demonstrate the applicability of the proposed controller on

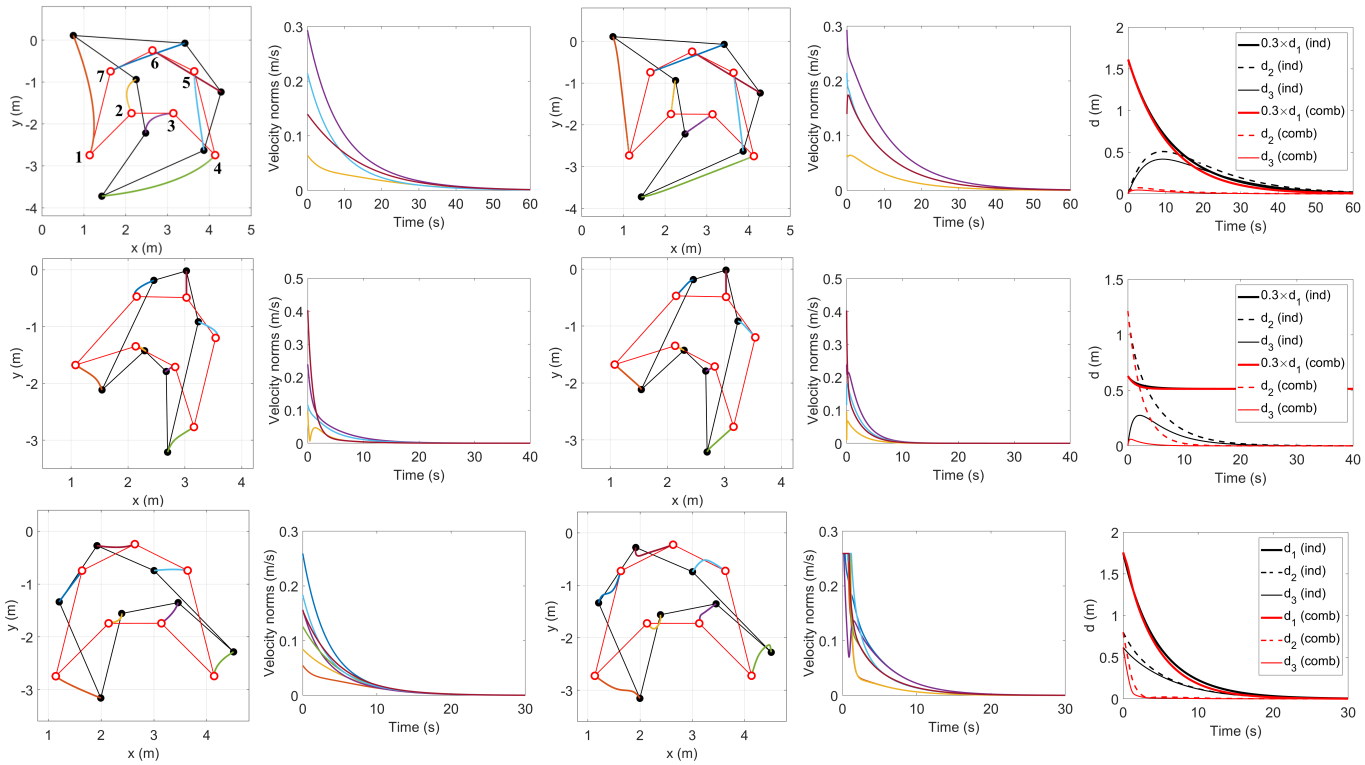

Fig. 2. Simulation results. Each row (1, 2, 3) corresponds to the scenario of the same number. For each row, the five plots from left to right are: robot paths (individual controller), robot velocity norms (individual controller), robot paths (combined controller), robot velocity norms (combined controller), and distances to formations. In the path plots, the initial positions are marked with solid circles and the final ones with hollow circles. For visualization purposes, several lines joining robot positions are shown to represent the outline of the initial and final configurations.

physical robots and under the non-ideal conditions and perturbations of a real-world scenario.

VI. Conclusion

We have presented a distributed control approach for planar multirobot formations based on combining individual controllers for different formation types. Notable features of our approach are its versatility and its ability to control the transient performance. We exemplified the latter by using the approach to execute efficient leaderless formation maneuvers. Future work directions include: (i) extending our design to other robot dynamics (e.g., unicycles), (ii) studying the robustness to noise, and (iii) addressing other team missions.

Appendix

Proof of Lemma 1: As $\mathbf{A}$ is real and symmetric, we can express $\mathbf{A} = \mathbf{U}\mathbf{D}\mathbf{U}^\intercal$ where $\mathbf{U}$ is orthogonal and its columns are the orthonormal eigenvectors of $\mathbf{A}$, and $\mathbf{D} = diag(\lambda_i)$ with $\lambda_i \in \mathbb{R}$, $\forall i \in \{1, ..., 2n\}$ the eigenvalues of $\mathbf{A}$ in increasing order. The system under the considered dynamics follows the trajectory $\mathbf{q}(t) = e^{\mathbf{A}t}\mathbf{q}(0)$. Note that $e^{\mathbf{A}t} = e^{\mathbf{U}(\mathbf{D}t)\mathbf{U}^\intercal} = \mathbf{U}e^{\mathbf{D}t}\mathbf{U}^\intercal$, where $e^{\mathbf{D}t} = diag(e^{\lambda_i t})$. λ_i are all real and non-positive as $\mathbf{A}$ is negative semidefinite.

If $\lambda_i < 0$, $e^{\lambda_i t} \to 0$ monotonically as $t \to \infty$, whereas if $\lambda_i = 0$, $e^{\lambda_i t} = 1^t = 1$ $\forall t$. Therefore, $||\mathbf{q}||$ remains bounded and, when $t \to \infty$, $e^{\mathbf{D}t} \to diag(0, ..., 0, 1, ..., 1)$. The number of ones, k, in this matrix is equal to the dimension of $\ker(\mathbf{A})$. Hence, when $t \to \infty$, $e^{\mathbf{A}t} \to \mathbf{P} = \mathbf{V}\mathbf{V}^\intercal$ where $\mathbf{V} \in \mathbb{R}^{2n \times k}$ contains the last k columns of $\mathbf{U}$ and is an orthonormal basis of $\ker(\mathbf{A})$. This means $\mathbf{P}$ is the orthogonal projection matrix onto $\ker(\mathbf{A})$. Hence, $\mathbf{q}(t \to \infty) = \mathbf{P}\mathbf{q}(0)$ is the orthogonal projection of $\mathbf{q}(0)$ onto that kernel. ■

Proof of Lemma 2: (i) Consider a $\mathbf{q} \in \mathbb{R}^{2n}$ such that $\mathbf{q} \in (\ker(\mathbf{A}) \cap \ker(\mathbf{B}))$. This implies $\mathbf{A}\mathbf{q} = \mathbf{0}$ and $\mathbf{B}\mathbf{q} = \mathbf{0}$, i.e., $(\mathbf{A} + \mathbf{B})\mathbf{q} = \mathbf{0}$. Hence, $\mathbf{q} \in \ker(\mathbf{A} + \mathbf{B})$. (ii) Consider a $\mathbf{q} \in \mathbb{R}^{2n}$ such that $\mathbf{q} \in \ker(\mathbf{A} + \mathbf{B})$. This implies $\mathbf{q}^\intercal(\mathbf{A}+\mathbf{B})\mathbf{q} = 0$, i.e., $\mathbf{q}^\intercal\mathbf{A}\mathbf{q}+\mathbf{q}^\intercal\mathbf{B}\mathbf{q} = 0$. Since $\mathbf{A}$ and $\mathbf{B}$ are symmetric negative semidefinite, this means $\mathbf{q}^\intercal\mathbf{A}\mathbf{q} = 0$ and $\mathbf{q}^\intercal\mathbf{B}\mathbf{q} = 0$. As $\mathbf{A}$ is symmetric negative semidefinite, there is a real symmetric positive semidefinite matrix $\mathbf{G}$ such that $\mathbf{A} = -\mathbf{G}^\intercal\mathbf{G}$. We can now see that $\mathbf{q}^\intercal\mathbf{A}\mathbf{q} = -\mathbf{q}^\intercal\mathbf{G}^\intercal\mathbf{G}\mathbf{q} = -||\mathbf{G}\mathbf{q}||^2 = 0$. This implies $\mathbf{G}\mathbf{q} = \mathbf{0}$, and $\mathbf{A}\mathbf{q} = -\mathbf{G}^\intercal\mathbf{G}\mathbf{q} = \mathbf{0}$. Therefore, $\mathbf{q} \in \ker(\mathbf{A})$. Using an identical reasoning, $\mathbf{q} \in \ker(\mathbf{B})$. Hence, $\mathbf{q} \in (\ker(\mathbf{A}) \cap \ker(\mathbf{B}))$. ■

Proof of Prop. 2: (i) Let us denote the n^2 blocks of size 2×2 of $\mathbf{A}^k$, $k \geq 0$, by $\mathbf{A}_{kij}$. Every such block has the form (12), from Assum. 3. Also, as $\mathbf{A}$ is symmetric (Assum. 1), $\mathbf{A}^k$ is symmetric for any integer $k \geq 0$. Defining $S_{ij} = \mathbf{c}_i^\intercal\mathbf{A}_{kij}\mathbf{S}\mathbf{c}_j \in \mathbb{R}$ for any two $i \in \mathcal{N}$, $j \in \mathcal{N}$, we can express

$$\mathbf{c}^\intercal\mathbf{A}^k\mathbf{T}\mathbf{c} = \sum_{\forall i} S_{ii} + \sum_{\forall i}\sum_{\forall j>i}(S_{ij} + S_{ji}). \tag{26}$$

As $\mathbf{A}^k$ is symmetric, for every block $\mathbf{A}_{kii}$ the two off-diagonal entries are necessarily zero, to satisfy the form (12). We thus have $\mathbf{A}_{kii} = a_{kii}\mathbf{I}_2$ for some $a_{kii} \in \mathbb{R}$, and hence $S_{ii} = \mathbf{c}_i^\intercal\mathbf{A}_{kii}\mathbf{S}\mathbf{c}_i = a_{kii}\mathbf{c}_i^\intercal\mathbf{S}\mathbf{c}_i = 0$ $\forall i$. For $i \neq j$, we write

$$S_{ji} = \mathbf{c}_j^\intercal\mathbf{A}_{kji}\mathbf{S}\mathbf{c}_i = (\mathbf{c}_j^\intercal\mathbf{A}_{kji}\mathbf{S}\mathbf{c}_i)^\intercal = \mathbf{c}_i^\intercal\mathbf{S}^\intercal\mathbf{A}_{kji}^\intercal\mathbf{c}_j. \tag{27}$$

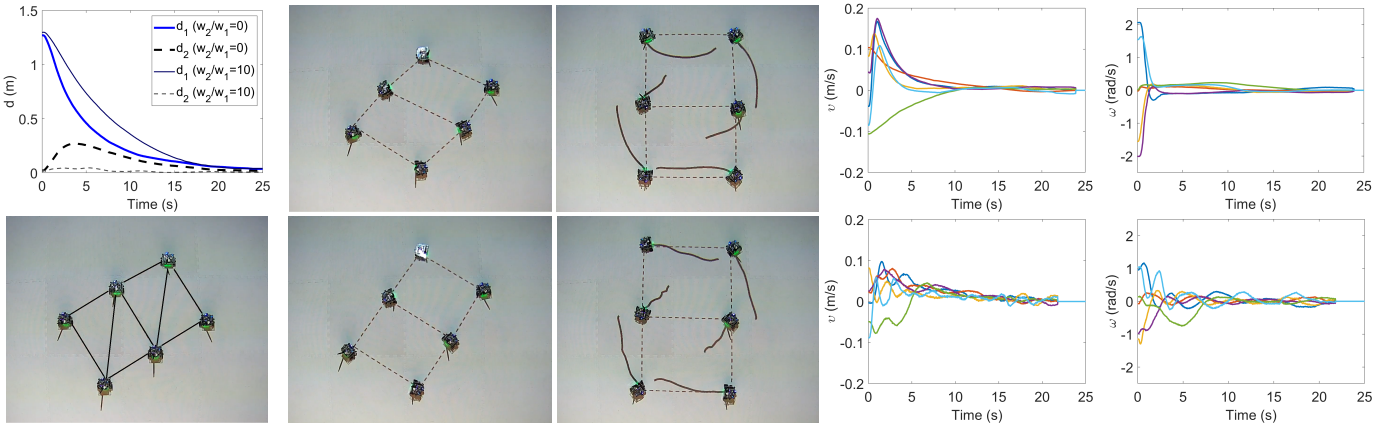

Fig. 3. Experimental results. Top-left: distances to formations. Bottom-left: initial configuration for the two tests, with the graph edges marked as solid lines. The remaining four plots in the first row are for the individual controller, and they show, from left to right: an intermediary configuration, final configuration with robot paths, linear and angular unicycle velocities. The remaining four plots in the second row are for the combined controller, and they show, from left to right: an intermediary configuration, final configuration with robot paths, linear and angular unicycle velocities.

We can apply on the rightmost term of (27) that $\mathbf{A}_{kji}^{\intercal} = \mathbf{A}_{kij}$ (due to symmetry of $\mathbf{A}^k$), and two identities that are easy to check: $\mathbf{S}^{\intercal} = -\mathbf{S}$ and $\mathbf{S}\mathbf{A}_{kij} = \mathbf{A}_{kij}\mathbf{S}$. One thus sees that $S_{ji} = -S_{ij}$. It follows from (26) that $\mathbf{c}^{\intercal}\mathbf{A}^k\mathbf{T}\mathbf{c} = 0$. As $e^{\mathbf{A}t}$ is a weighted sum of the powers $\mathbf{A}^k$, we conclude that $\mathbf{c}^{\intercal}e^{\mathbf{A}t}\mathbf{T}\mathbf{c} = 0$. Transposing and noting that $e^{\mathbf{A}t}$ is symmetric (because $\mathbf{A}$ is symmetric), we see $(\mathbf{T}\mathbf{c})^{\intercal}e^{\mathbf{A}t}\mathbf{c} = 0$ too.

(ii) Notice $(\mathbf{T}\mathbf{c})^{\intercal}e^{\mathbf{A}t}\mathbf{T}\mathbf{c} = \mathbf{c}^{\intercal}(\mathbf{T}^{\intercal}e^{\mathbf{A}t}\mathbf{T})\mathbf{c}$. Recall that $\mathbf{T} = \mathbf{I}_n \otimes \mathbf{S}$, i.e., $\mathbf{T}$ is block-diagonal with every 2×2 diagonal block equal to $\mathbf{S}$. Then, notice every block (i, j) of size 2×2 of $\mathbf{A}^k\mathbf{T}$ (respectively, $\mathbf{T}\mathbf{A}^k$) is equal to $\mathbf{A}_{kij}\mathbf{S}$ (respectively, $\mathbf{S}\mathbf{A}_{kij}$). Since, as noted above, $\mathbf{A}_{kij}\mathbf{S} = \mathbf{S}\mathbf{A}_{kij}$, we have $\mathbf{A}^k\mathbf{T} = \mathbf{T}\mathbf{A}^k$. Therefore, $e^{\mathbf{A}t}\mathbf{T} = \mathbf{T}e^{\mathbf{A}t}$, and $\mathbf{T}^{\intercal}e^{\mathbf{A}t}\mathbf{T} = \mathbf{T}^{\intercal}\mathbf{T}e^{\mathbf{A}t}$. Noticing that $\mathbf{T}^{\intercal}\mathbf{T} = \mathbf{I}_{2n}$, the result follows. ■

REFERENCES

[1] K.-K. Oh, M.-C. Park, and H.-S. Ahn, "A survey of multi-agent formation control," *Automatica*, vol. 53, pp. 424–440, 2015.

[2] H. Garcia de Marina, B. Jayawardhana, and M. Cao, "Distributed rotational and translational maneuvering of rigid formations and their applications," *IEEE Trans. Rob.*, vol. 32, no. 3, pp. 684–697, 2016.

[3] M. H. Trinh, S. Zhao, Z. Sun, D. Zelazo, B. D. O. Anderson, and H.-S. Ahn, "Bearing-based formation control of a group of agents with leader-first follower structure," *IEEE Transactions on Automatic Control*, vol. 64, no. 2, pp. 598–613, 2019.

[4] C. J. Stamouli, C. P. Bechlioulis, and K. J. Kyriakopoulos, "Multi-agent formation control based on distributed estimation with prescribed performance," *IEEE Robotics and Automation Letters*, vol. 5, no. 2, pp. 2929–2934, 2020.

[5] R. Olfati-Saber, J. A. Fax, and R. M. Murray, "Consensus and cooperation in networked multi-agent systems," *Proceedings of the IEEE*, vol. 95, no. 1, pp. 215–233, 2007.

[6] D. V. Dimarogonas and K. J. Kyriakopoulos, "A connection between formation infeasibility and velocity alignment in kinematic multi-agent systems," *Automatica*, vol. 44, no. 10, pp. 2648–2654, 2008.

[7] E. Nuño, A. Loría, T. Hernández, M. Maghenem, and E. Panteley, "Distributed consensus-formation of force-controlled nonholonomic robots with time-varying delays," *Autom.*, vol. 120, p. 109114, 2020.

[8] Z. Lin, L. Wang, Z. Han, and M. Fu, "Distributed formation control of multi-agent systems using complex Laplacian," *IEEE Transactions on Automatic Control*, vol. 59, no. 7, pp. 1765–1777, 2014.

[9] K. Fathian, S. Safaoui, T. H. Summers, and N. R. Gans, "Robust distributed planar formation control for higher order holonomic and nonholonomic agents," *IEEE Transactions on Robotics*, vol. 37, no. 1, pp. 185–205, 2021.

[10] M. Aranda, G. López-Nicolás, and Y. Mezouar, "Distributed linear control of multirobot formations organized in triads," *IEEE Robotics and Automation Letters*, vol. 6, no. 4, pp. 8498–8505, 2021.

[11] Z. Lin, L. Wang, Z. Chen, M. Fu, and Z. Han, "Necessary and sufficient graphical conditions for affine formation control," *IEEE Trans. Autom. Control*, vol. 61, no. 10, pp. 2877–2891, 2016.

[12] S. Zhao, "Affine formation maneuver control of multiagent systems," *IEEE Trans. Autom. Control*, vol. 63, no. 12, pp. 4140–4155, 2018.

[13] L. Chen, J. Mei, C. Li, and G. Ma, "Distributed leader–follower affine formation maneuver control for high-order multiagent systems," *IEEE Trans. Autom. Control*, vol. 65, no. 11, pp. 4941–4948, 2020.

[14] R. Herguedas, M. Aranda, G. López-Nicolás, C. Sagüés, and Y. Mezouar, "Multirobot control with double-integrator dynamics and control barrier functions for deformable object transport," in *2022 Int. Conf. on Robotics and Automation (ICRA)*, 2022, pp. 1485–1491.

[15] ——, "Double-integrator multirobot control with uncoupled dynamics for transport of deformable objects," *IEEE Robotics and Automation Letters*, forthcoming, 2023.

[16] M. Aranda, J. Sanchez, J. A. Corrales Ramon, and Y. Mezouar, "Robotic motion coordination based on a geometric deformation measure," *IEEE Systems Journal*, vol. 16, no. 3, pp. 3689–3699, 2022.

[17] Y. Lin, Z. Lin, Z. Sun, and B. D. O. Anderson, "A unified approach for finite-time global stabilization of affine, rigid, and translational formation," *IEEE Transactions on Automatic Control*, vol. 67, no. 4, pp. 1869–1881, 2022.

[18] K. Fathian, D. I. Rachinskii, M. W. Spong, T. H. Summers, and N. R. Gans, "Distributed formation control via mixed barycentric coordinate and distance-based approach," in *Amer. Contr. Conf.*, 2019, pp. 51–58.

[19] M. Deghat, B. D. O. Anderson, and Z. Lin, "Combined flocking and distance-based shape control of multi-agent formations," *IEEE Trans. Autom. Control*, vol. 61, no. 7, pp. 1824–1837, 2016.

[20] F. Mehdifar, F. Hashemzadeh, M. Baradarannia, and M. de Queiroz, "Finite-time rigidity-based formation maneuvering of multiagent systems using distributed finite-time velocity estimators," *IEEE Transactions on Cybernetics*, vol. 49, no. 12, pp. 4473–4484, 2019.

[21] X. Fang, X. Li, and L. Xie, "Distributed formation maneuver control of multiagent systems over directed graphs," *IEEE Transactions on Cybernetics*, vol. 52, no. 8, pp. 8201–8212, 2022.

[22] L. Chen, H. Garcia de Marina, and M. Cao, "Maneuvering formations of mobile agents using designed mismatched angles," *IEEE Transactions on Automatic Control*, vol. 67, no. 4, pp. 1655–1668, 2022.

[23] H. Garcia de Marina, "Distributed formation maneuver control by manipulating the complex Laplacian," *Automatica*, vol. 132, p. 109813, 2021.

[24] S. Wilson, P. Glotfelter, L. Wang, S. Mayya, G. Notomista, M. Mote, and M. Egerstedt, "The Robotarium: Globally impactful opportunities, challenges, and lessons learned in remote-access, distributed control of multirobot systems," *IEEE Control Systems Magazine*, vol. 40, no. 1, pp. 26–44, 2020.